

Обзор ArXiv/astro-ph,  
1-13 февраля 2021 года

От Сильченко О.К.

# ArXiv: 2102.02449

- **The Fornax3D project: Assembly histories of lenticular galaxies from a combined dynamical and population orbital analysis**
- A. Poci, R. M. McDermid, M. Lyubenova, L. Zhu, G. van de Ven, E. Iodice, L. Coccato, F. Pinna,
- E. M. Corsini, J. Falcon-Barroso, D. A. Gadotti, R. J. J. Grand, K. Fahrion, I. Martin-Navarro,
- M. Sarzi, S. Viaene, P. T. de Zeeuw

# Исследуемые галактики

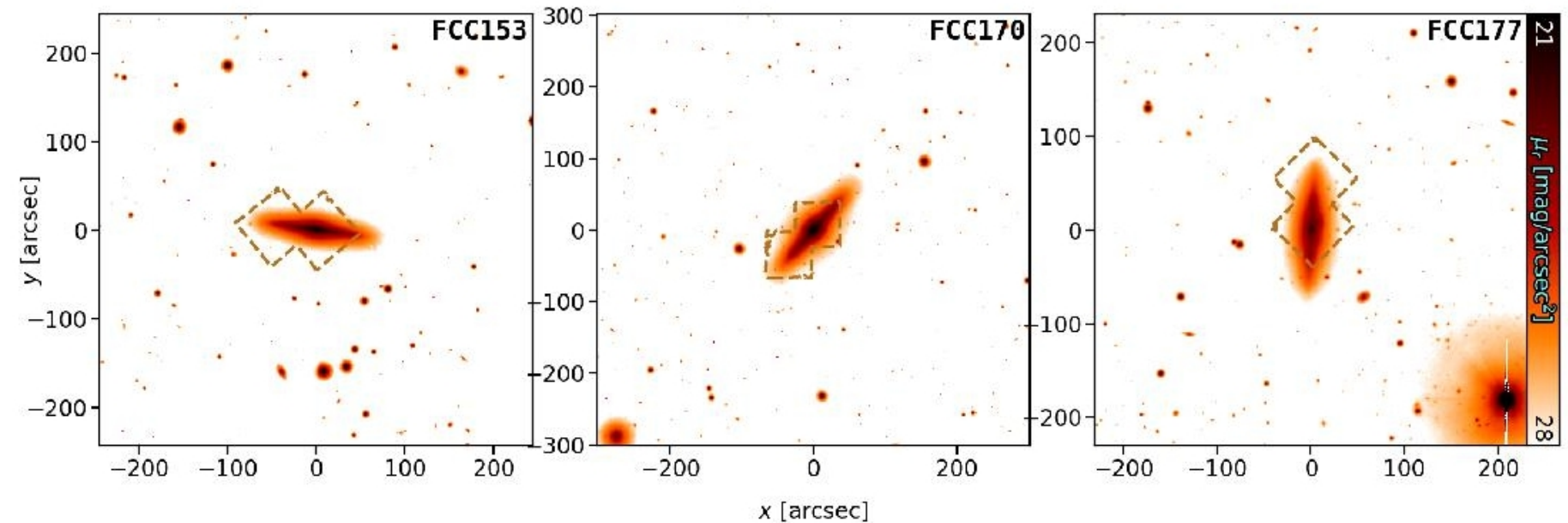


**Fig. 2.** Full  $r$ -band images from FDS, overlaid with the MUSE FOV in dashed brown for FCC 153 (*left*), FCC 170 (*middle*), and FCC 177 (*right*).

**IC 335**

**NGC 1381**

**NGC 1380A**

# Галактики и их фазовые диаграммы

Galaxy	$D$ [Mpc]	$R_c$	$M_e^*$ [ $\log_{10} M_\odot$ ]	$M_e^{DM}$ [ $\log_{10} M_\odot$ ]	$R_{enc}$	$M_{enc}^*$ [ $\log_{10} M_\odot$ ]	$M_{enc}^{DM}$ [ $\log_{10} M_\odot$ ]
(1)	(2)	(3)	(4)	(5)	(6)	(7)	(8)
FCC 153	20.8	19.80'' 2.00 kpc	9.55	9.63	165.78'' 16.72 kpc	10.06	11.43
FCC 170	21.9	15.90'' 1.69 kpc	10.33	8.83	148.39'' 15.76 kpc	10.67	10.74
FCC 177	20.0	35.90'' 3.48 kpc	9.43	9.71	133.347'' 12.93 kpc	9.73	10.84

**Table 1.** (1) the galaxy name. (2) distance to the galaxy (3) the  $r$ -band effective radius taken from Iodice et al. (2019b) and converted into physical units at our adopted distances. (3) – (4) the stellar and DM masses enclosed within  $R_c$ , respectively. (5) the radius at which the enclosed stellar mass asymptotes (c.f. Fig. 3). (6) – (7) the stellar and DM masses enclosed within  $R_{enc}$ , respectively.

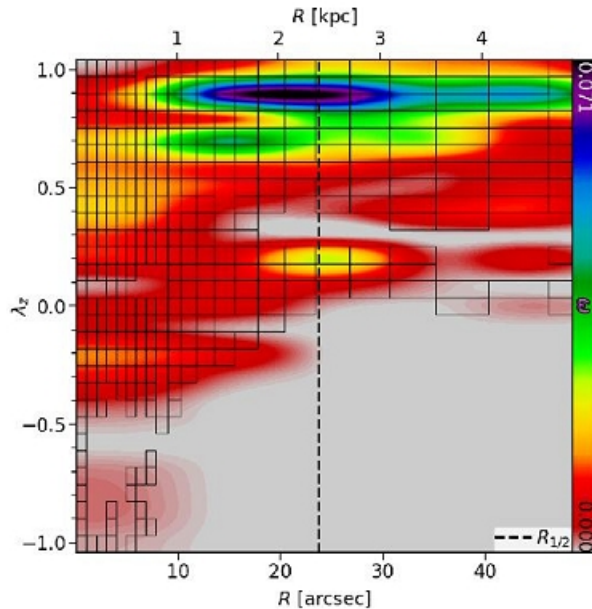


**Fig. 4.** Phase-space of circularity  $\lambda_z$  as a function of cylindrical radius  $R$  for the best-fit model of FCC 153. The colour represents the orbital weight from the Schwarzschild model, which has been normalised to an integral of unity. The dynamical decomposition is overlaid in black.

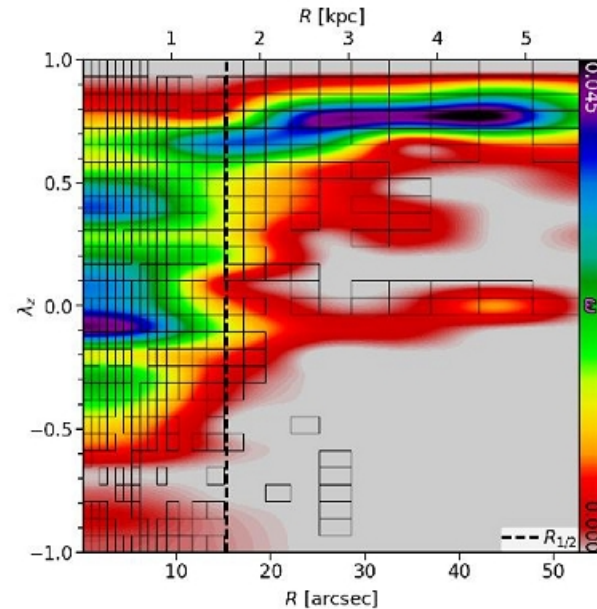


**Fig. 5.** Same as Fig. 4, but for FCC 170. This galaxy has a large contribution from hot central orbits, with most of the cold orbits appearing at larger radius.

# Результаты для полей MUSE

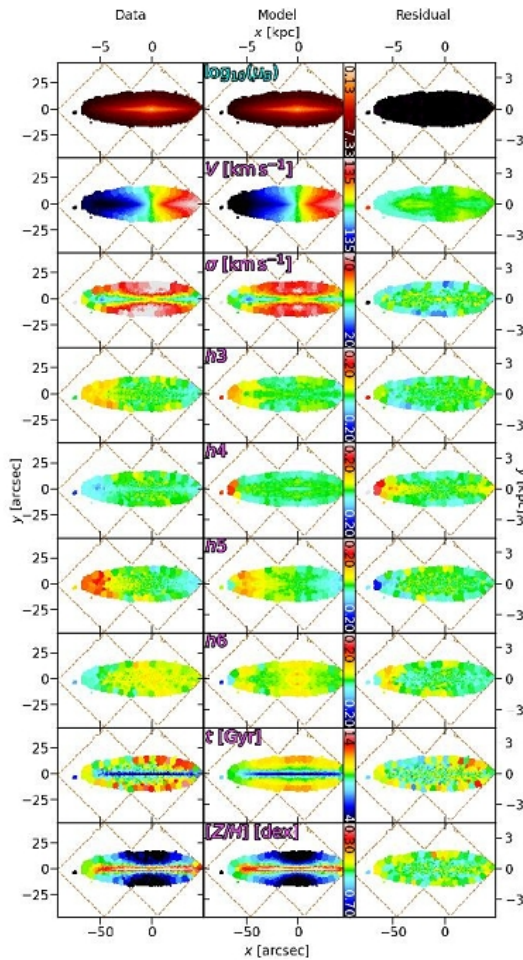


Fig. 7. Best-fitting Schwarzschild model for FCC 153. The data (left), fits (middle), and residuals (right) of, from top to bottom, the dynamical model (surface brightness, velocity, velocity dispersion, and  $h3 - h6$ ), and the subsequent stellar-population fitting (age and metallicity). The

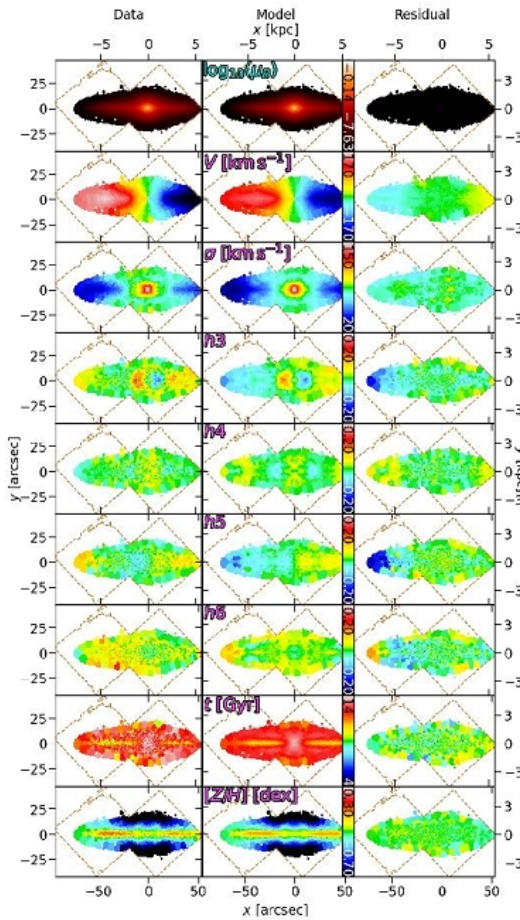


Fig. 8. Same as Fig. 7, but for FCC 170.

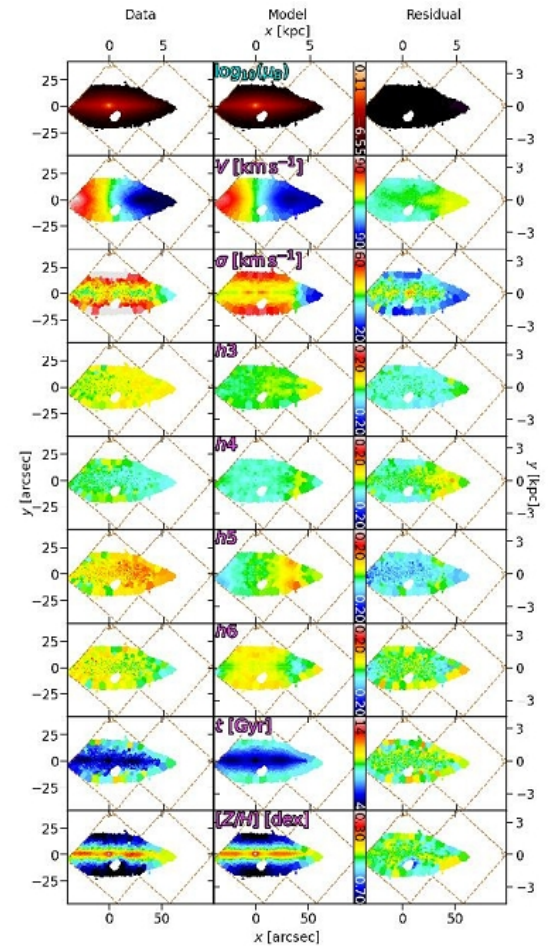
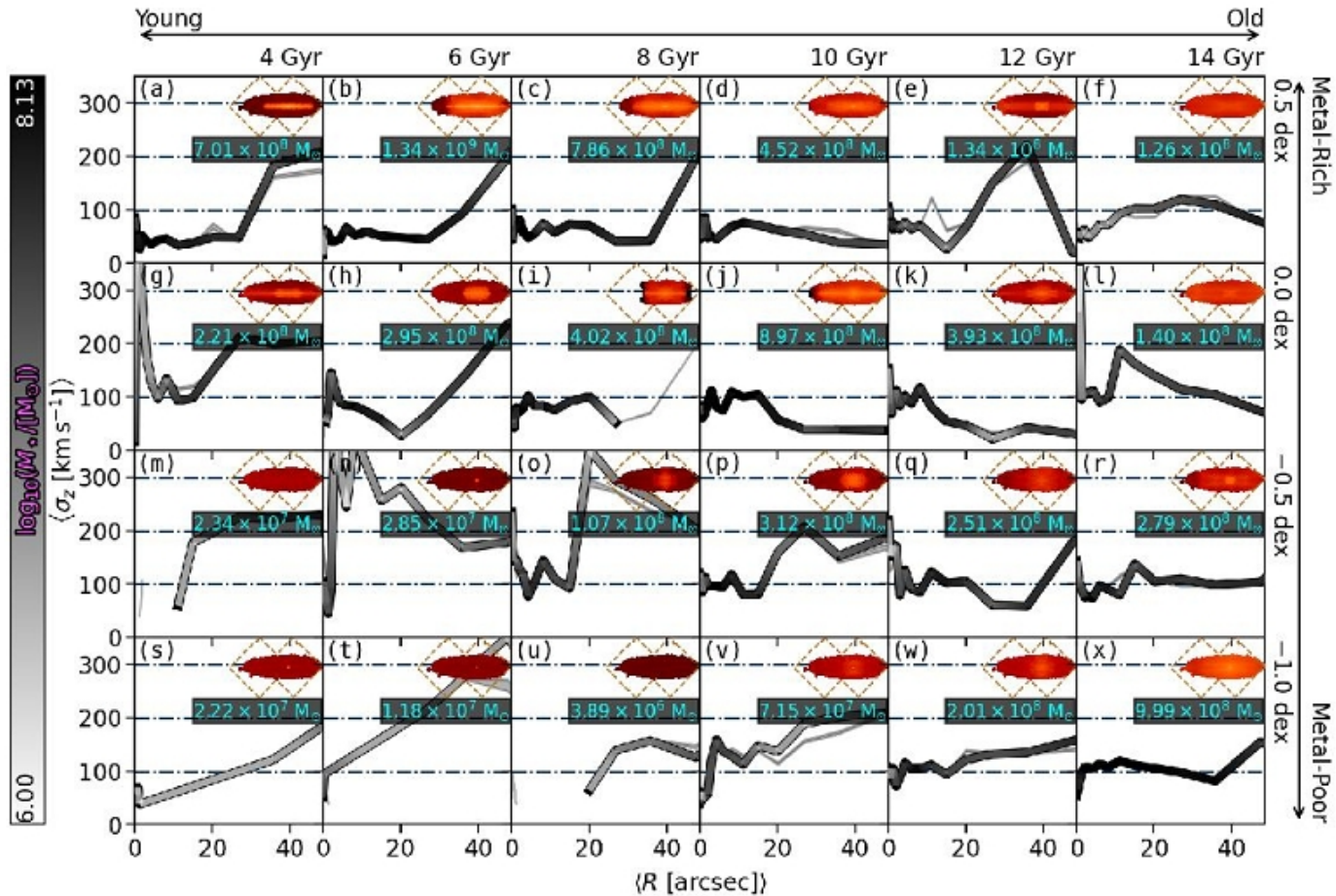


Fig. 9. Same as Fig. 7, but for FCC 177.

# «Сборка» IC 335



**Fig. 10.** Mass assembly history for FCC 153. The panels are ordered by increasing mean stellar age (*left to right*) and decreasing mean stellar metallicity (*top to bottom*). The value given at the top and right of each column and row, respectively, denotes its upper bound (inclusive). Each panel is composed of a radial profile of the vertical stellar velocity dispersion  $\sigma_z$  (*black/white curve*), the surface brightness distribution at the best-fitting projection (*top-right*) with the outline of the MUSE mosaic shown in dashed brown, and the total stellar mass within the FOV for that panel. The  $\sigma_z(R)$  profiles are coloured according to the stellar mass in that panel at that radius (sampled within the logarithmic radial bins). This indicates the spatial region in which each curve contributes most (white regions), and which regions may be impacted by numerical noise (black regions). The grey shaded regions show the spread of velocity dispersion profiles for 100 Monte Carlo fits to the stellar-population maps. This galaxy exhibits a dominant disk-like, metal-rich component that has steadily formed over the last  $\sim 10$  Gyr.

# «Сборка» NGC 1381

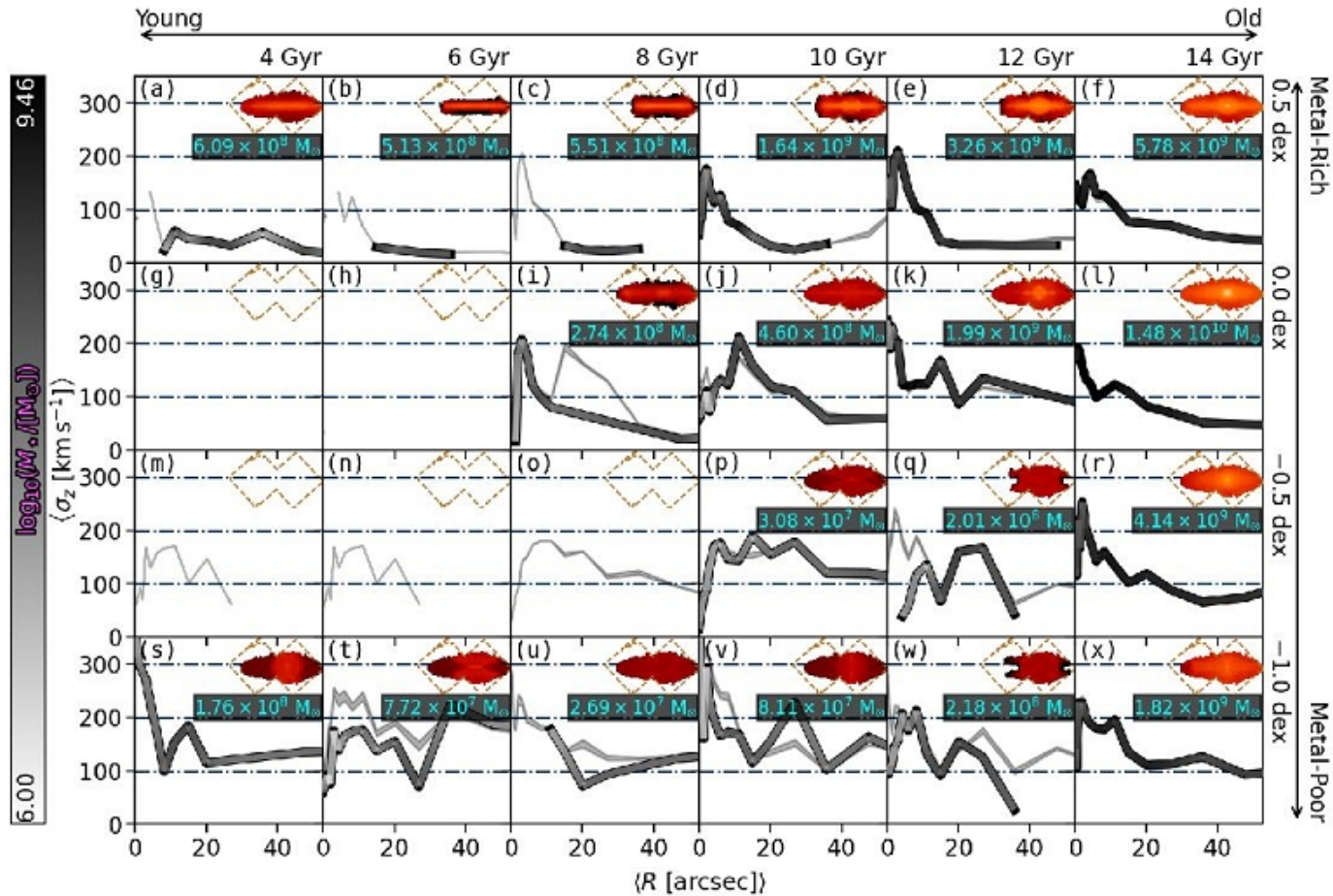


**Fig. 11.** Same as Fig. 10, but for FCC 170. This galaxy is dominated by an old central pressure-supported spheroidal component spanning  $\sim 1$  dex in metallicity. It has a secondary contribution from a progressively thinner and younger disk-like component, and a potential minor contribution from a warm metal-poor halo-like component.

# «Сборка» NGC 1380A

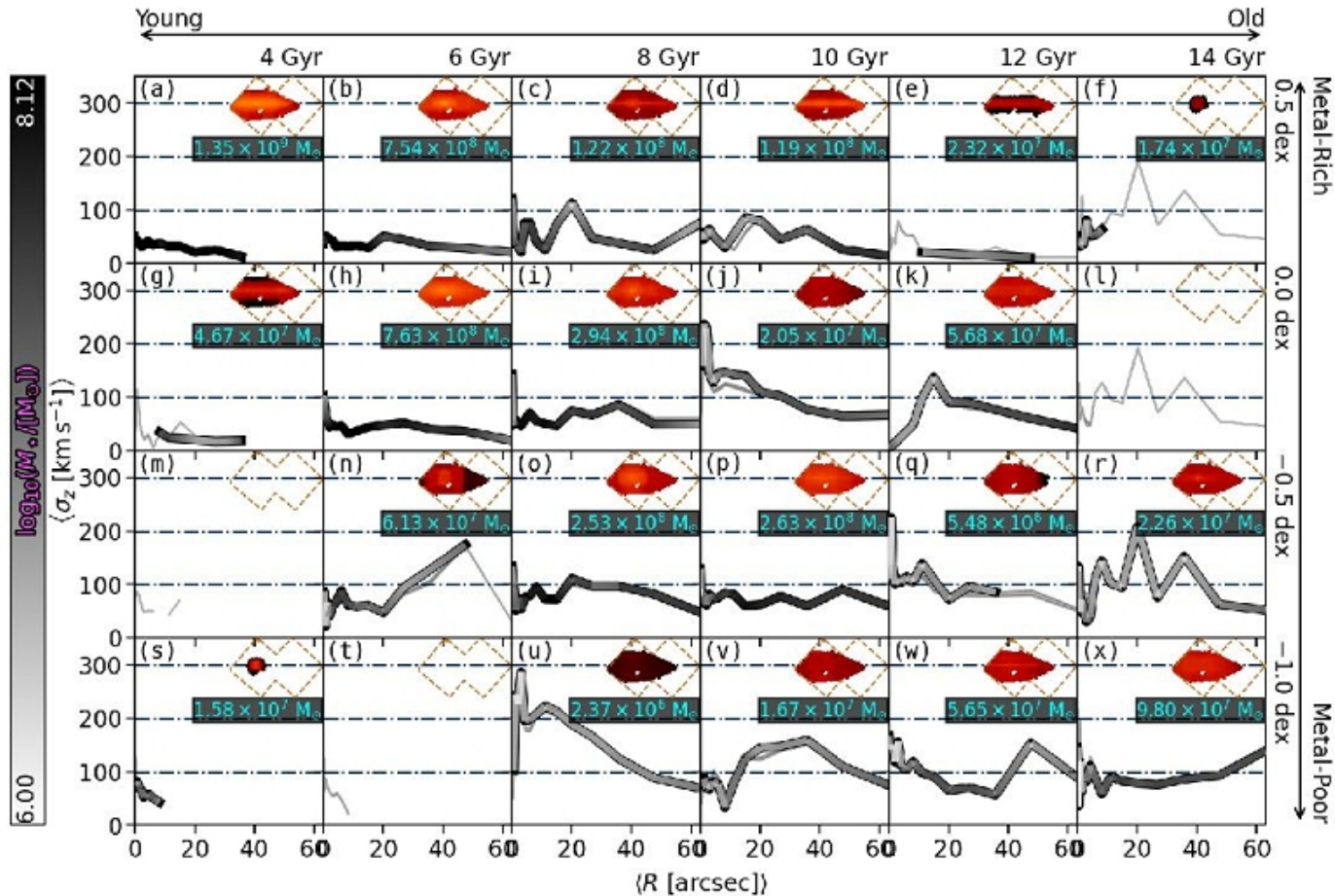
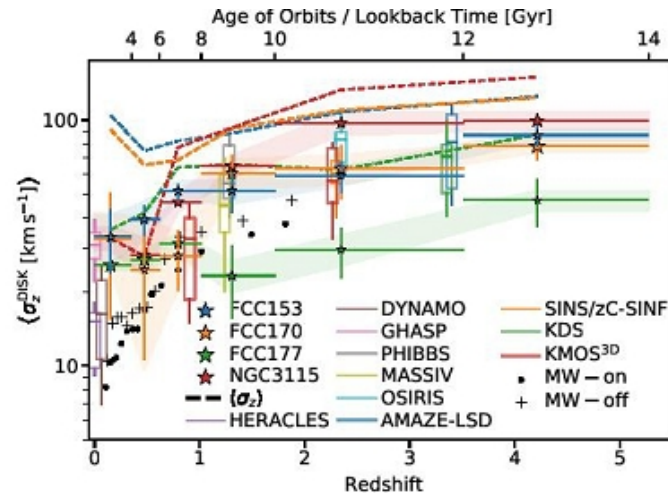


Fig. 12. Same as Fig. 10, but for FCC 177. This galaxy appears to have begun forming late. It is dominated by a young, thin disk, with contributions from dynamically-warmer and slightly older stars.



# Формирование толстых дисков из турбулентного газа?



**Fig. 13.** Stellar disk AVR as derived from our models. The coloured stars are the galaxies modelled in this work (and Poci et al. 2019, for NGC 3115). The symbol size is proportional to the fractional stellar mass in each age bin, for each galaxy independently. The horizontal error-bars denote the width of the age bin. The vertical error bars are computed as the weighted standard deviation within each age bin, for the best-fit model. The shaded regions show the spread in  $\sigma_z$  for 100 Monte Carlo fits to the stellar-population maps. The dashed curves show the stellar AVR of the four S0 galaxies when all orbits are included (no selection on orbital circularity). The box-whisker plots are literature measurements of cold gas disks, from HERACLES (Leroy et al. 2009), DYNAMO (Green et al. 2014), GHASP (Epinat et al. 2010), PHIBBS (Tacconi et al. 2013), MASSIV (Epinat et al. 2012), OSIRIS (Law et al. 2009), AMAZE-LSD (Gnerucci et al. 2011), SINS (Schreiber et al. 2009) and zC-SINF (Schreiber et al. 2014), KMOS<sup>3D</sup> (Wisnioski et al. 2015), and KDS (Turner et al. 2017). The black dots and crosses are Milky-Way stellar measurements (Yu & Liu 2018) for stars on ( $|z| < 270$  pc) and off ( $|z| > 270$  pc) the plane, respectively. Galaxy disks become dynamically colder towards the present day. The cluster S0 galaxies have a higher contribution from warmer orbits at more recent times compared to the field galaxy (comparing the full and disk-only  $\sigma_z$ ). The Milky-Way, despite its higher stellar mass, is dynamically colder than the S0 galaxies studied here.

# ArXiv: 2102.05957

## A massive stellar bulge in a regularly rotating galaxy 1.2 billion years after the Big Bang

Federico Lelli,<sup>1,2,\*</sup> Enrico M. Di Teodoro<sup>3</sup>, Filippo Fraternali<sup>4</sup>, Allison W.S. Man<sup>5</sup>,  
Zhi-Yu Zhang<sup>6</sup>, Carlos De Breuck<sup>7</sup>, Timothy A. Davis<sup>1</sup>, Roberto Maiolino<sup>8,9</sup>

<sup>1</sup>School of Physics and Astronomy, Cardiff University, Cardiff CF24 3AA, UK

<sup>2</sup>Arcetri Astrophysical Observatory, INAF, Florence 50125, Italy; \*e-mail: federico.elli@inaf.it

<sup>3</sup>Department of Physics & Astronomy, Johns Hopkins University, Baltimore MD 21218, USA

<sup>4</sup>Kapteyn Astronomical Institute, University of Groningen, Groningen 9700 AV, The Netherlands

<sup>5</sup>Dunlap Institute for Astronomy & Astrophysics, University of Toronto, Toronto ON M5S 3H4, Canada

<sup>6</sup>School of Astronomy and Space Science, Nanjing University, Nanjing 210023, P.R. China

<sup>7</sup>European Southern Observatory, Germany Headquarters, Garching bei München 85748, Germany

<sup>8</sup>Kavli Institute for Cosmology, University of Cambridge, Cambridge CB3 0HA, UK

<sup>9</sup>Cavendish Laboratory, University of Cambridge, Cambridge CB3 0HE, UK

# SMG на $z=4.75$ с разрешением $0.11''$

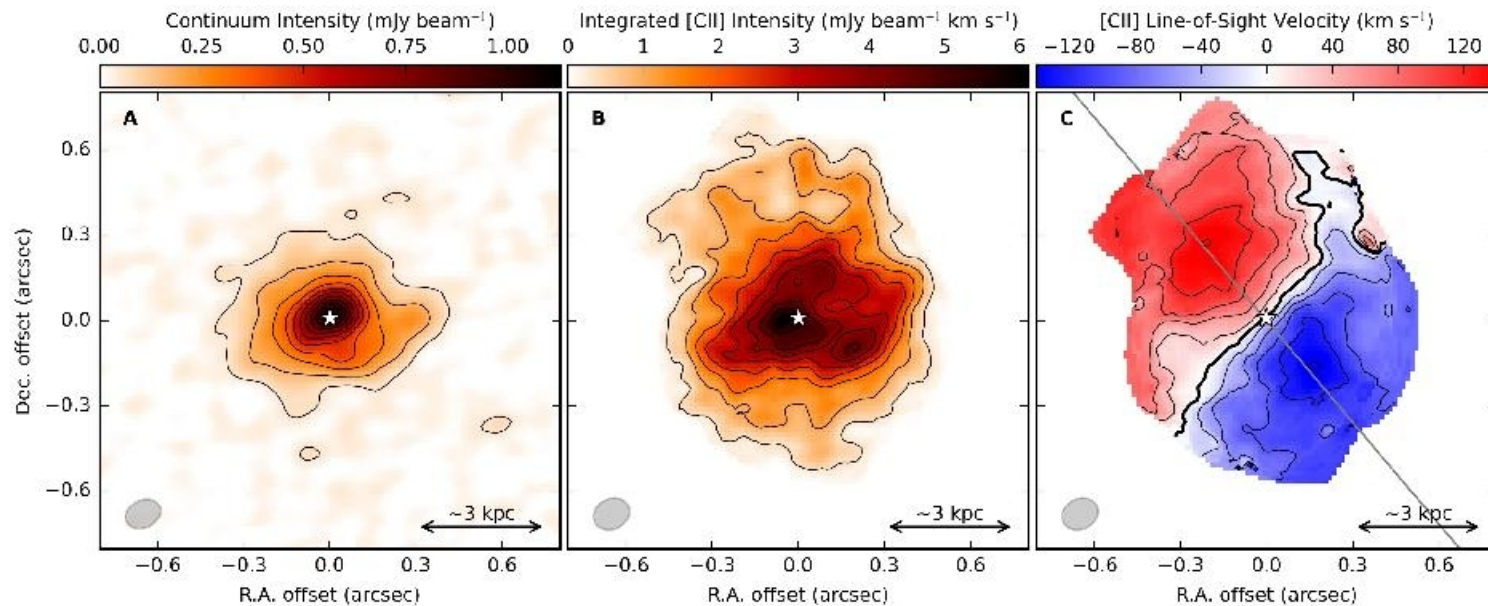
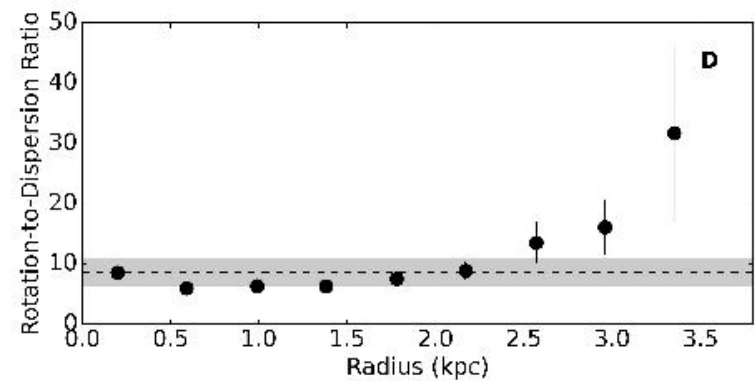
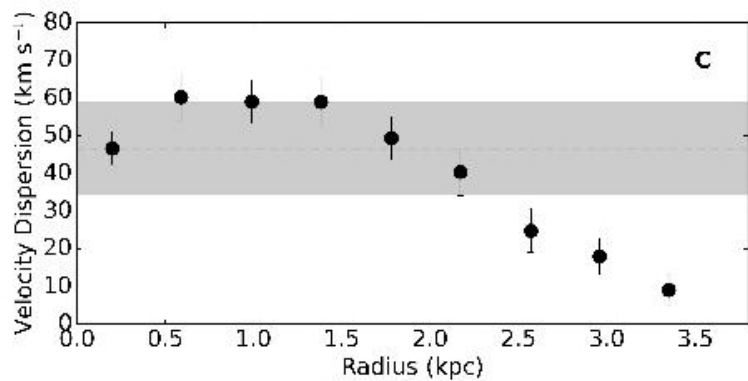
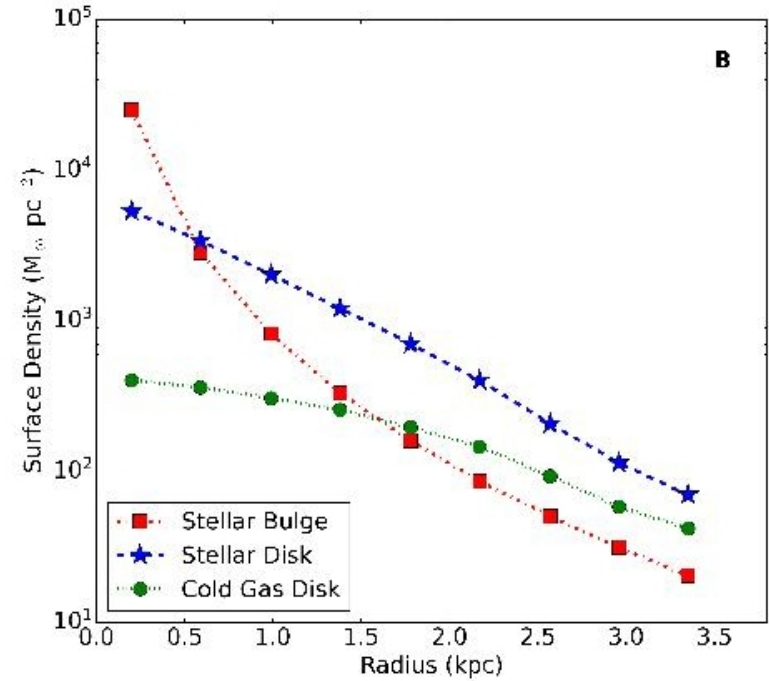
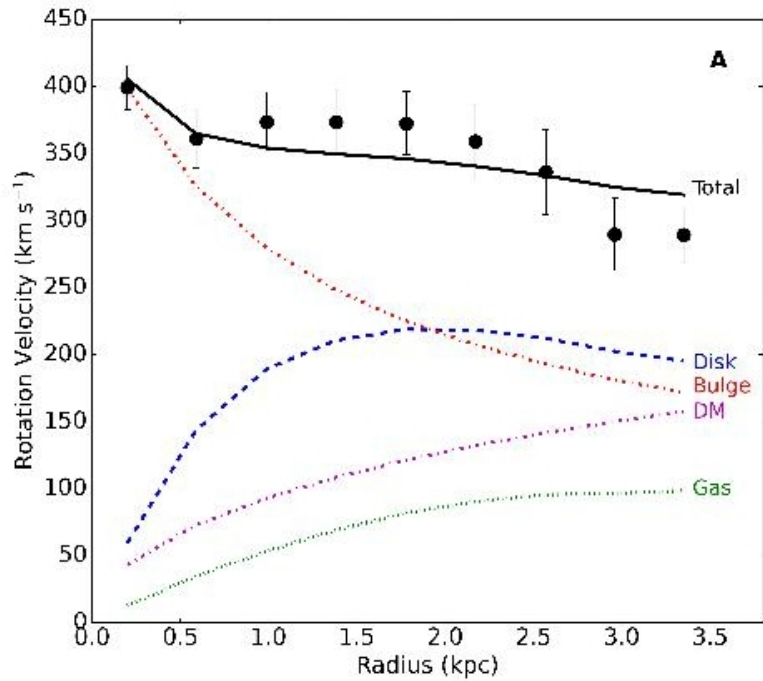


Figure 1: **ALMA observations of ALESS 073.1.** (A) Continuum emission at  $160 \mu\text{m}$  (rest-frame) tracing dust heated by young stars, (B) [C II] intensity map tracing cold gas, and (C) [C II] velocity field showing a rotating disk. North is up and east is left. The kinematic center, located at a Right Ascension (R.A.) of  $03^{\text{h}} 32^{\text{m}} 29.295^{\text{s}}$  and Declination (Dec.) of  $-27^{\circ} 56' 19.60''$ , is represented by a white star. The beam size is plotted as the grey ellipse in the bottom-left corner. The physical scale is indicated by the scale bar in the bottom-right corner. In (A), iso-emission contours range from  $0.055$  to  $1 \text{ mJy beam}^{-1}$  (where  $1 \text{ mJy} = 10^{-29} \text{ W m}^{-2} \text{ Hz}^{-1}$ )

# Динамическая модель



# Альтернативные модели (например, без балджа) не проходят

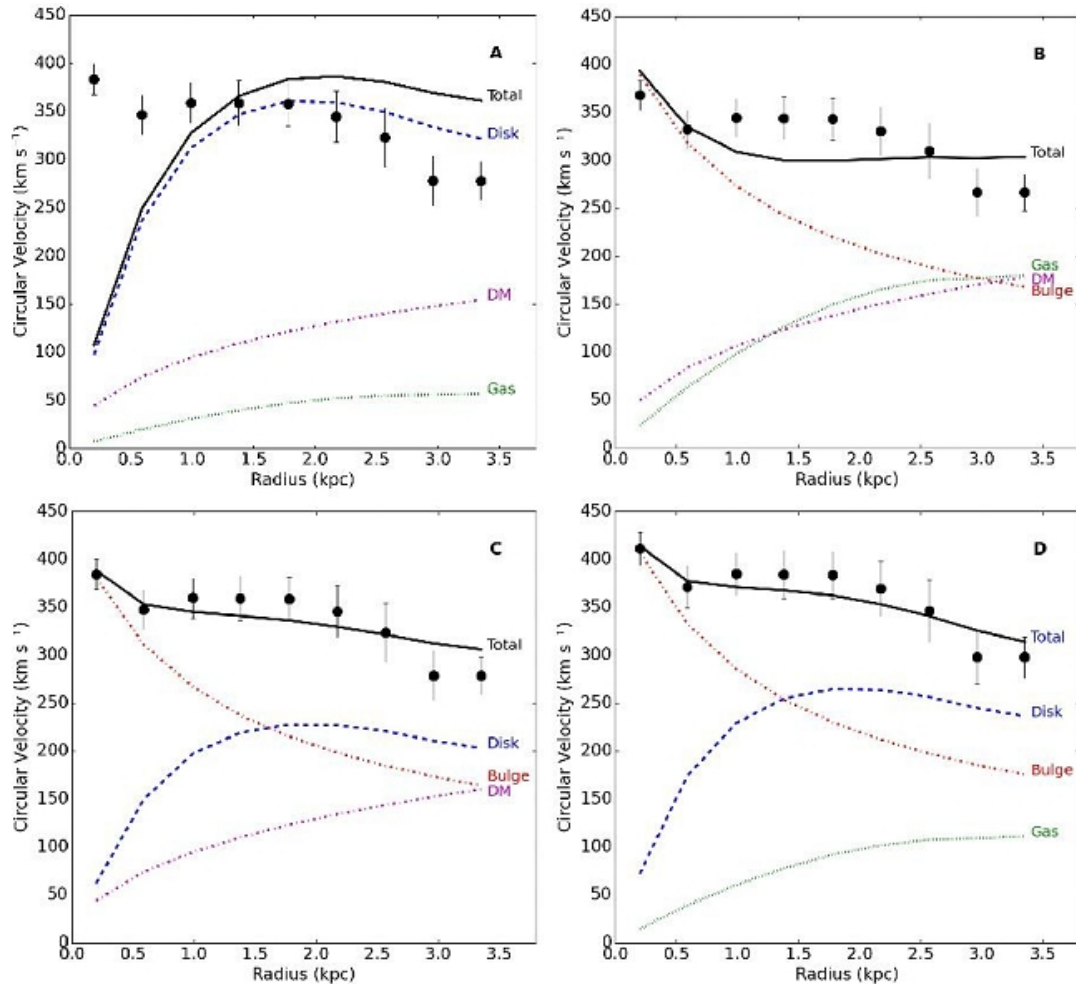


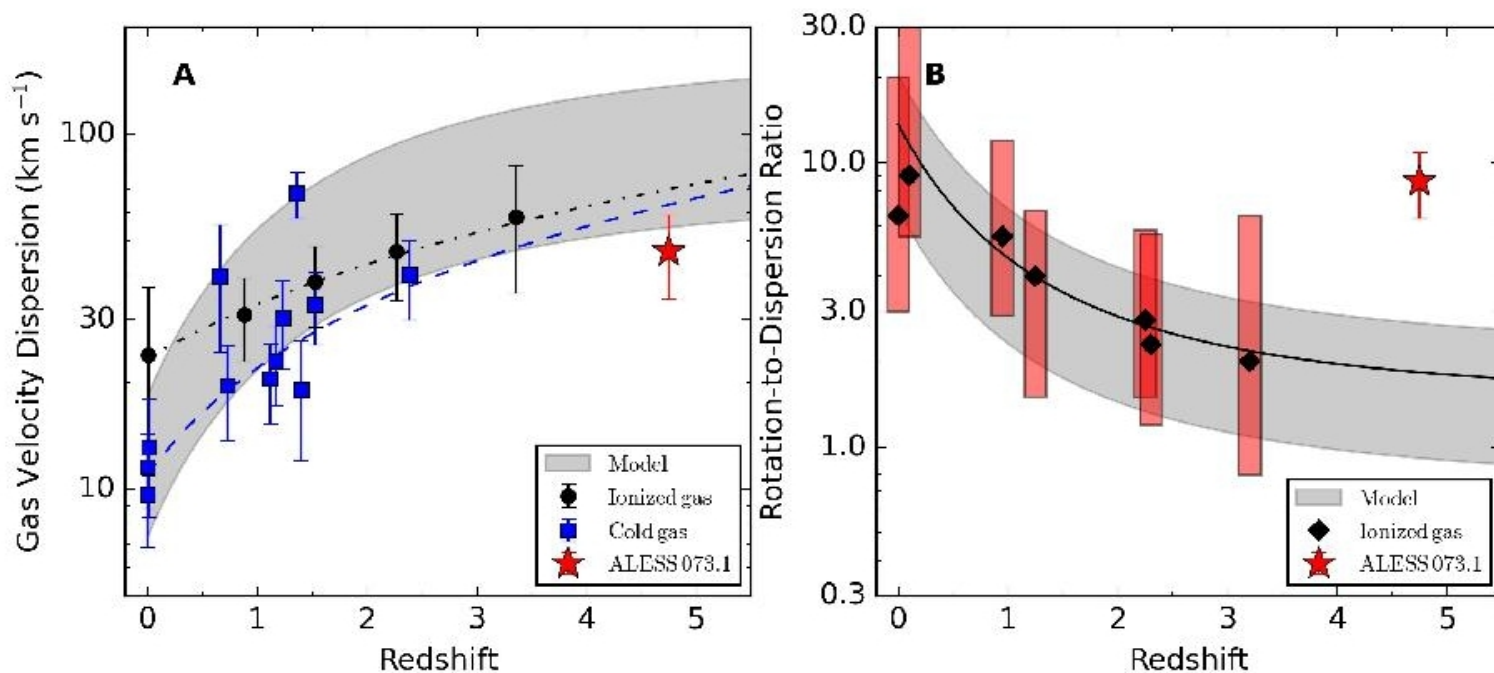
Figure S6: **Alternative Mass Models:** the observed rotation curve (black dots) is compared

# Параметры best-fit

Table S2: MCMC results. The uncertainties correspond to  $1\sigma$  confidence regions (see Fig. S5).

$i$ ( $^\circ$ )	$22.0^{+2.9}_{-2.9}$
$M_{\text{gas}}$ ( $10^{10} M_\odot$ )	$0.5^{+0.4}_{-0.4}$
$M_{\text{disk}}$ ( $10^{10} M_\odot$ )	$2.4^{+0.9}_{-1.0}$
$M_{\text{bul}}$ ( $10^{10} M_\odot$ )	$2.3^{+0.6}_{-0.6}$
$V_{200}$ ( $\text{km s}^{-1}$ )	$263^{+81}_{-80}$
$C_{200}$	$2.9^{+0.9}_{-0.9}$
$M_{200}$ ( $10^{11} M_\odot$ )	$8.1^{+2.7}_{-2.7}$
$M_{\text{baryon}}$ ( $10^{10} M_\odot$ )	$5.2^{+1.2}_{-1.2}$
$M_{\text{bul}}/M_{\text{baryon}}$	$0.44^{+0.11}_{-0.12}$

# Что же с эволюцией динамической температуры диска??



# Холодный диск → спиральные рукава?

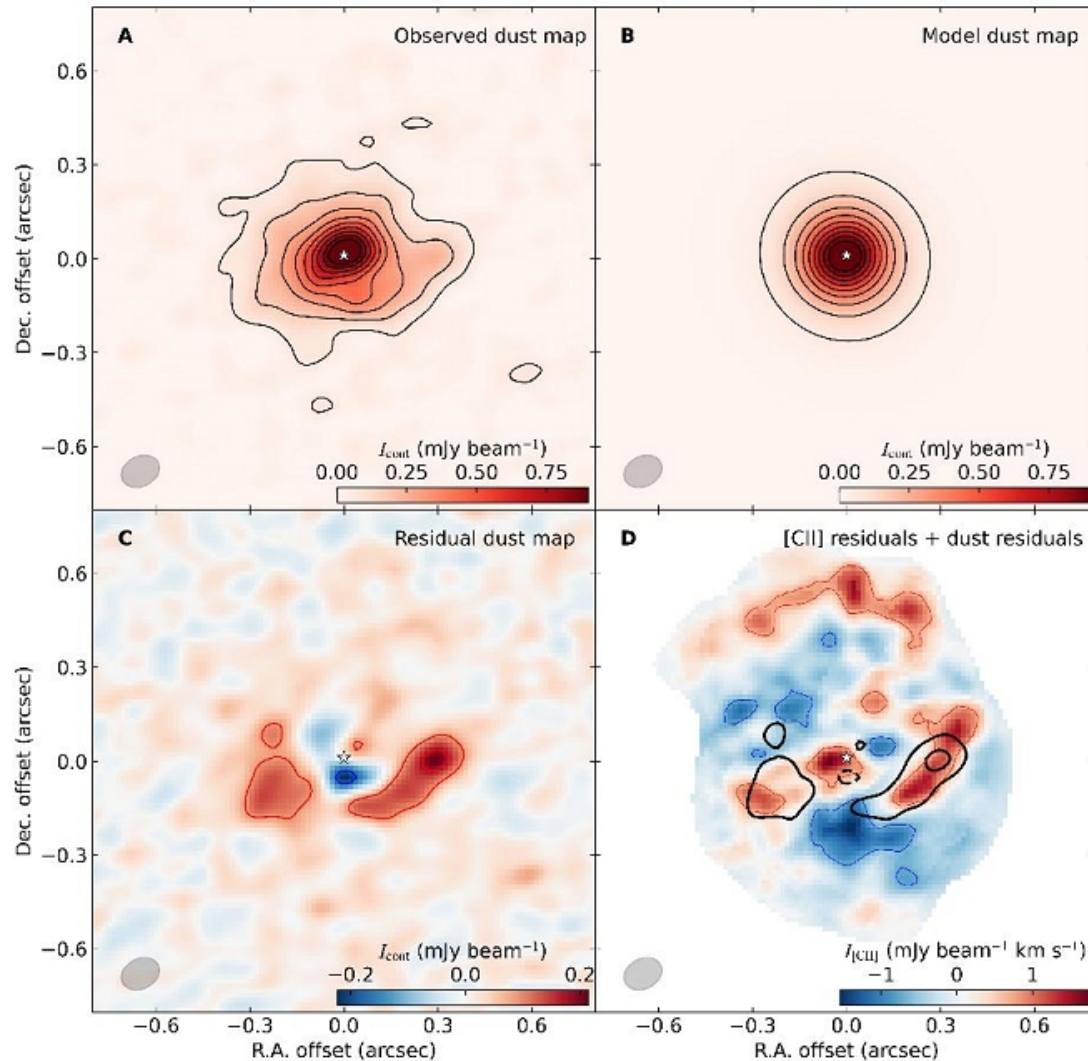


Figure S4: Dust Distributions: observed continuum intensity ( $I_{\text{cont}}$ ) map at rest from 160  $\mu\text{m}$